Electronic Supplementary Information

Expanding the solid-state landscape of dexamethasone: a specific sandwich structure in facilitating the formation of kinetically stable cocrystals from mechanochemistry

Si Nga Wong[1, #], Kam-Hung Low[2, #], Jingwen Weng[1], Ho Wan Chan[1], Shing Fung Chow[1, 3*]

[1] Department of Pharmacology and Pharmacy, Li Ka Shing Faculty of Medicine, The University of Hong Kong, Pokfulam, Hong Kong SAR, China

[2] Department of Chemistry, Faculty of Science, The University of Hong Kong, Pokfulam, Hong Kong SAR, China

[3] Advanced Biomedical Instrumentation Centre, Hong Kong Science Park, Shatin, Hong Kong SAR, China

# S.N.W. and K.H.L. contributed equally

EXPERIMENTAL SECTION

Materials. DEX (≥99%) was obtained from Yick Vic Chemicals & Pharmaceuticals Limited (Hong Kong, China). The benzenediols and benzenetriols as coformers including catechol (CAT), resorcinol (RES), hydroquinone (HYQ), hydroxyquinol (HXQ), phloroglucinol (PHL), and pyrogallol (PYR) were purchased from Sigma-Aldrich (St. Louis, MO, USA) and Alfa Aesar (Ward Hill, MA, USA). Potassium bromide (KBr) for FTIR analysis was sourced from J&K Scientific Limited, China. Sodium chloride (NaCl), potassium chloride (KCl), and calcium chloride ($CaCl_2$) for preparation of simulated nasal fluid were obtained from VWR BDH Chemicals (VWR International S.A.S., France). Ethanol and methanol of analytical grade were obtained from VWR BDH Chemicals (VWR International S.A.S., France) and Merck KGaA (Darmstadt, Germany). Water was purified through a Thermolyne NANOpure Diamond Analytical ultra-pure water system (Barnstead, Thermo Fisher Scientific, Waltham, MA, USA).

Preparation of DEX Cocrystals. Attempts to cocrystallize DEX with benzenediol (CAT, RES, and HYQ) and benzenetriol coformers (HXQ, PHL, and PYG) were made using neat grinding, solution evaporation, and melt crystallization. For neat grinding, equimolar amounts (0.597 mmol) of DEX (234.3 mg) and benzenediol (65.7 mg) were mixed and ground with a mortar and pestle for approximately 15 min at ambient temperature. The powders were frequently scraped out from the mortar and pestle, and re-mixed throughout the grinding process. Prior to solid-state characterizations, the variation of particle size was minimized by passing the samples through a standard testing sieve with a diameter of 63 μm (VWR International, New York, USA). For solution evaporation, equimolar amounts (0.597 mmol) of DEX (234.3 mg) and the coformer (65.7 mg) were dissolved in a beaker with 100 mL ethanol (EtOH), methanol (MeOH), acetone (ACE), and acetonitrile (ACN), respectively, followed by sonication until a homogeneous solution was obtained. The solutions were sealed with pierced parafilm to allow for slow evaporation in a fumehood for 72h. Rapid solvent removal was performed by a rotary evaporator (Buchi, Germany) under a vacuum with the rotary flask being immersed in a water bath at 60 °C with a rotating speed of 60 rpm. The product was dried in an oven at 60 °C for 3h to remove residual solvent and gently triturated to a fine powder for further analysis. For melt crystallization, a physical mixture of DEX and coformer in 1:1 molar ratio was heated at 10°C/min until a melt was formed using a differential scanning calorimeter. The molten mixture was then cooled to designated temperatures at a cooling

rate of 10°C/min. The mixture was kept at the annealing temperature until the crystallization process was completed, up to 24h. All the resulting products were stored in sealed containers until further analysis.

Powder X-Ray Diffraction (PXRD) and Crystal Structure Determination. The polycrystalline cocrystals of DEX were characterized by X-ray diffraction. The measurements were done on a Rigaku SmartLab 9kW diffractometer with a copper rotating anode (K alpha1 1.54059 Å, K alpha2 1.54441 Å) rated at 200 mA/ 45 kV at room temperature with a step size of 0.02 degree two-theta. Bragg Brentano CBO incident X-ray optics was used, with a 5.0 deg incident parallel Soller slit, a 1/2 degree incident slit, a 1.0 x 10.0 mm length limiting slit, a 5.0 deg receiving parallel slit, a 1/2 degree first receiving slit and a 0.3 mm second receiving slit. Diffraction signals were filtered with a K beta nickel filter, and diffraction data were collected with a HyPix-3000 detector in 1D mode. Possible unit cell parameters were obtained by N-TREOR09[1] based on the diffraction patterns. Unit cells with reasonable volumes were used for further analysis. Space group determination was done by detecting the extinction group. The three-dimensional atomic coordinates of the individual components, CAT[2], RES[3], and DEX[4] are known in the literature. These atomic coordinates were used as the initial models for the simulated annealing procedures in the EXPO2014 program suite[5]. Ten simulated annealing with ten structure solutions generated in each annealing were made for a consistent converging structure model. The structures with the lowest cost function were used for Rietveld refinement (**Fig. S10**). All non-hydrogen atoms were refined isotropically. Geometrical restraints were applied on the DEX, CAT, RES molecules according to the reported crystal structures of the individual compounds, but not on the alpha-hydroxy ketone group in DEX. Hydrogen atoms were included in the idealized positions. Selected crystallographic data and structure refinement results are shown in **Table S6**.

Thermal Analysis. Differential scanning calorimetry (DSC) and thermogravimetric analysis (TGA) profiles were generated by a TA DSC 250 differential scanning calorimeter (TA Instruments, New Castle, DE, USA) and a TGA Q5000 thermogravimetric analyzer (TA Company, New Castle, DE, USA), respectively. For DSC experiments, pure indium was used for routine calibration of enthalpy and cell constant. An accurately weighed sample (~3 mg) was encased in a Tzero Aluminum Hermetic pan (TA Instruments, New Castle, DE, USA) with pinhole vented

lid if required and heated from 50°C to 300°C at a scanning rate of 10°C/min. In the TGA experiments, each sample (5–7 mg) was placed on an open pan and heated at 10°C/min from 50 °C to 300 °C. Nitrogen was used as the purge gas at 20 mL/min for both the DSC and TGA analyses. The TA Trios Software was used for data analysis.

Fourier-Transform Infrared Spectroscopy (FTIR). The FTIR spectra were obtained with a FTIR spectrophotometer (Spectrum Two, PerkinElmer Instrument, USA) in a KBr diffuse reflectance mode. The scan was performed in the range of 4000 cm^{-1} to 400 cm^{-1} at an interval 0.5 cm^{-1}. A total of 32 scans were collected at a resolution of 4 cm^{-1} for each sample.

Scanning Electron Microscopy (SEM). The particle morphology of the samples was observed by field emission scanning electron microscopy (Hitachi S-4800 FEG, Hitachi, Tokyo, Japan). The powders were sprinkled onto carbon adhesive tape mounted on SEM stubs. Any sample not adhering to the tape was removed by compressed air. A sputter coater (Bal-tec SCD 005 Sputter Coater, Bal-Tec GmbH, Schalksmühle, Germany) was used to coat the powder with approximately 11 nm gold-palladium alloy in two cycles (60 s each) to create a conductive layer and avoid overheating.

High Performance Liquid Chromatography (HPLC). The concentrations of DEX were quantified by HPLC equipped with a diode array detector (Agilent 1200 series, Agilent Technologies, USA) and an Agilent Zorbax Eclipse Plus C18 column (5 μm, 250 mm × 4.6 mm) in an isocratic condition at 239 nm. The mobile phase consisted of a mixture of methanol and water (65:35, v/v). A 30 μL aliquot of each sample solution was injected onto the column with a flow rate of 1 mL/min. The retention time of DEX was found at 8.3 min.

Particle Size Distribution Measurement by Laser Diffraction. The particle size and size distribution of the powders was determined using laser diffraction equipment, Mastersizer 3000 (Malvern Instruments Ltd, Worcestershire, UK) with Aero S dry powder disperser. Prior to the analysis, both raw DEX and DEX cocrystals powders were sifted with a diameter under 63 μm to control the particle size variation. The particle size distribution was calculated from the light scattering pattern using Mie theory. Particle size at 10% (D_{10}), 50% (D_{50}), 90% (D_{90}) of the volume

distribution were calculated automatically using the Mastersizer 3000 software based on Fraunhofer theory. Span was calculated as $(D_{90} - D_{10})/D_{50}$. All the samples were measured in triplicate.

***In-Vitro* Drug Release Study.** To study the drug release profile of the cocrystal systems, a previously reported method was adopted with slight modifications[6-8]. 1.5 mg of raw DEX powders and equimolar amount of sieved DEX cocrystal powders were separately poured into a jacketed beaker containing 50 mL of pH 5.5 simulated nasal fluid (8.77 g NaCl, 2.98 g KCl, 0.59 g $CaCl_2$ and distilled water made up to 1000 ml), for a period of 120 min at 37±0.5°C under sink condition. The solution was stirred at 50 rpm on a magnetic stirrer. The dissolution medium and temperature were selected to mimic the physiological condition in the nasal cavity[9, 10]. At designated time points of 5, 10, 15, 20, 30, 45, 60, 90, and 120 min, 1 mL of the dissolution medium was withdrawn and replaced with an equal volume of fresh medium. The sample solution was filtered through 0.45 μm nylon syringe filters and assayed for drug content by the HPLC. The intrinsic dissolution rate (IDR) is determined by the following equation: $IDR = (dm/dt)_{max}/A$, where $(dm/dt)_{max}$ is the slope of the initial linear region of the cumulative dissolution curve until 10% of drug is dissolved, and A is the specific surface area of the dissolution sample. The following assumptions were made: (i) spherical particles, (ii) constant particle size, and (iii) constant number of particles during the initial phase of the dissolution experiment under sink condition. With the assumptions, the particle size distribution data collected by laser diffractometry is used for the particle surface area ($SA_{particle}$) calculation. The total number of particles (n) subject to dissolution is calculated by $V_{bulk}/V_{particle}$, where $V_{particle}$ is the volume of each primary particle, and V_{bulk} is the volume of compound added to the dissolution medium. The total surface area of all particles added to the dissolution medium is thus calculated through $nSA_{particle}$. Finally, the specific surface area (A, m^2/g) defined as the total surface area of a material per unit of mass could be obtained.

Apparent Solubility. Apparent solubility test of DEX cocrystals was performed by adding excess solid in screw capped test tubes with 2 mL of distilled water, simulated nasal fluid, and ethanol, respectively, and shaking for 3 h. The solution was filtered to collect the undissolved solids, followed by air-drying and thermal analysis through DSC.

Stability Study. To assess the stability under moisture stress, raw DEX and DEX cocrystal powders were stored at 25 °C/75% RH for 1 month. The samples before and after the storage were collected for PXRD analysis. The assay of drugs was quantified by HPLC.

Statistical Analysis. A two-sample t-test was employed for data analysis. A p-value less than 0.05 was considered as statistically significant.

Table S1. Drug assay before and after storage of the DEX-benzenediol cocrystal systems under 25°C/75% RH in day 0, 7, and 30.

Compound	Time Interval	% of DEX Remaining (n = 3)	% Difference (Day 0 - Day 30)
DEX	Day 0	98.77 ± 2.97	4.27 ± 5.14 (p=0.23)
	Day 7	97.23 ± 4.27	
	Day 30	94.50 ± 3.00	
DEX-CAT	Day 0	97.83 ± 2.32	2.38 ± 5.49 (p=0.46)
	Day 7	96.73 ± 4.72	
	Day 30	95.45 ± 3.35	
DEX-RES	Day 0	99.65 ± 2.58	4.50 ± 4.07 (p=0.19)
	Day 7	97.18 ± 3.87	
	Day 30	95.15 ± 3.17	

Table S2. Melting temperature and heat of fusion of DEX, the polyphenolic coformers, and each DEX cocrystal systems (n = 3).

Sample	Melting point (°C)	ΔH_f (kJ/mol)
DEX	273.8 ± 0.5	42.9 ± 1.5
CAT	104.9 ± 0.3	28.5 ± 0.2
RES	109.7 ± 0.6	22.1 ± 0.2
DEX-CAT	128.9 ± 1.1	26.8 ± 0.3
DEX-RES	137.5 ± 0.8	18.0 ± 1.5

Table S3. Key features in the FTIR spectra of DEX, the polyphenolic coformers, and each DEX cocrystal systems.

Sample	O−H stretching /cm^{-1}	C=O stretching /cm^{-1}	C=C stretching /cm^{-1}
DEX	3472	1662	1618, 1603
CAT	3451, 3329	---	1599
RES	3261	---	1609
DEX-CAT	3555, 3466, 3201	1662	1616, 1603
DEX-RES	3555, 3470, 3260	1662	1618, 1603

Table S4. Interaction energies (kJ/ mol), the scale factor values, and distance between molecular centroids R (Angstroms) of the DEX-CAT and DEX-RES cocrystal systems. DEX/CAT is the nearest pair of DEX and CAT molecules; DEX/RES is the nearest pair of DEX and RES molecules; 3 CAT is the summation of the values of three CAT molecules in close proximity; 3 RES is the summation of the values of three RES molecules in close proximity. All computations were performed with CrystalExplorer 21.5 using HF/3-21G monomer electron densities[11].

Molecules		k_{ele}	k_{pol}	k_{disp}	k_{rep}	
		1.019	0.651	0.901	0.811	
	R	E_{ele}	E_{pol}	E_{disp}	E_{rep}	E_{tot}
DEX/CAT	8.95	-92.5	-29.7	-13.4	115.5	-31.9
DEX/RES	8.55	-88.7	-29.0	-11.5	91.1	-45.7
3 CAT	5.90/ 6.11	-48.6	-15.2	-16.1	44.5	-37.8
3 RES	6.10/ 6.79	-15.8	-2.2	-14.6	3.0	-28.2

Table S5. The volumetric size distribution of DEX, and each DEX cocrystal system measured by laser diffraction (n=3).

Formulations	Volumetric size (μm)			
	D_{10}	D_{50}	D_{90}	Span
DEX	0.93 ± 0.16	1.52 ± 0.50	2.76 ± 1.54	3.15 ± 0.46
DEX-CAT	8.49 ± 1.76	24.87 ± 6.75	49.27 ± 6.42	5.14 ± 0.28
DEX-RES	4.46 ± 1.93	12.0 ± 0.42	35.03 ± 8.92	7.69 ± 0.93

Table S6. Selected crystallographic data and structure refinement results of DEX-CAT and DEX-RES.

	DEX-CAT	DEX-RES
Moiety formula	$C_{22}H_{29}FO_5$, $C_6H_6O_2$	$C_{22}H_{29}FO_5$, $C_6H_6O_2$
Formula weight	502.576	502.576
Crystal system	Monoclinic	Monoclinic
Space group	$P2_1$	$P2_1$
Temperature/ K	293	293
Appearance	White powder	White powder
a/Å	16.9895(7)	18.9012(7)
b/Å	6.1074(2)	6.10485(19)
c/Å	12.0498(9)	22.6364(15)
α/°	90	90
β/°	101.833(6)	109.250(4)
γ/°	90	90
Volume/Å^3	1223.73(11)	2465.9(2)
Z	2	4
ρ_{calc}/gcm^3	1.364	1.354
$2\theta_{min}$, $2\theta_{max}$ /°	3.00, 59.960	3.00, 69.94
$2\theta_{step}$ /°	0.02	0.02
Number of reflections	410	1239
Final R_{wp}/ R_{exp}/ R_I	0.076/0.034/0.092	0.087/0.035/0.093

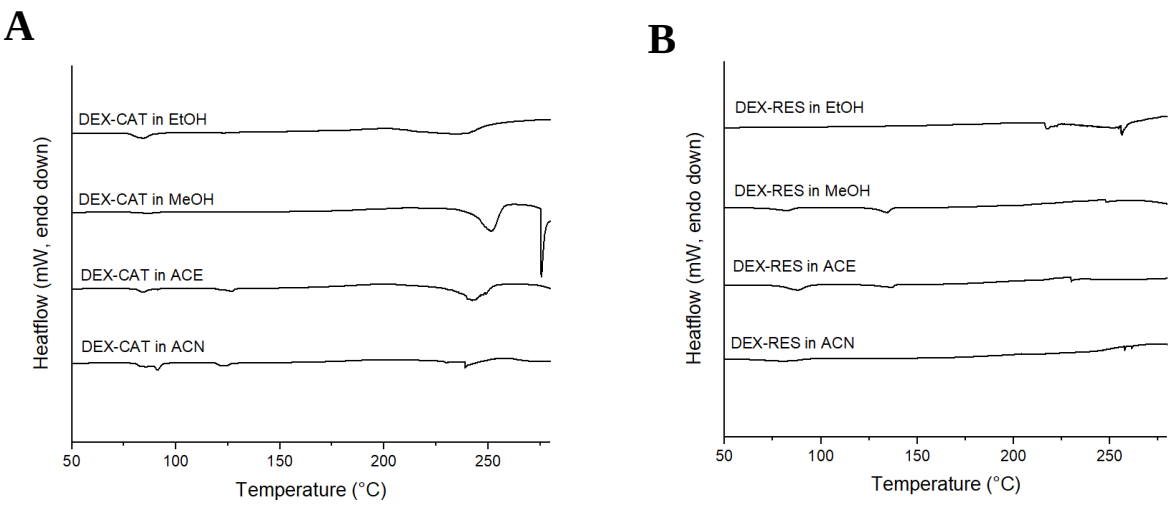

Fig. S1 DSC profiles of (A) DEX-CAT, and (B) DEX-RES samples produced via slow evaporation in different organic solvents.

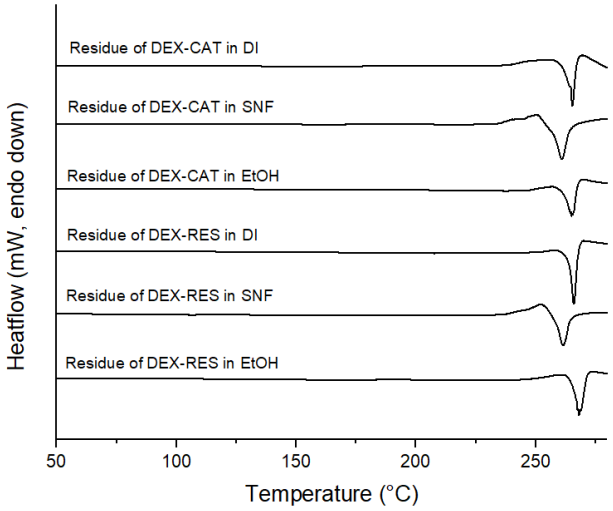

Fig. S2 DSC profiles of the residue DEX collected after a 3-hour apparent solubility study. DEX-CAT and DEX-RES failed to sustain their cocrystal form in aqueous solution (i.e., distilled water, simulated nasal fluid, and ethanol), indicative of their kinetically stable nature.

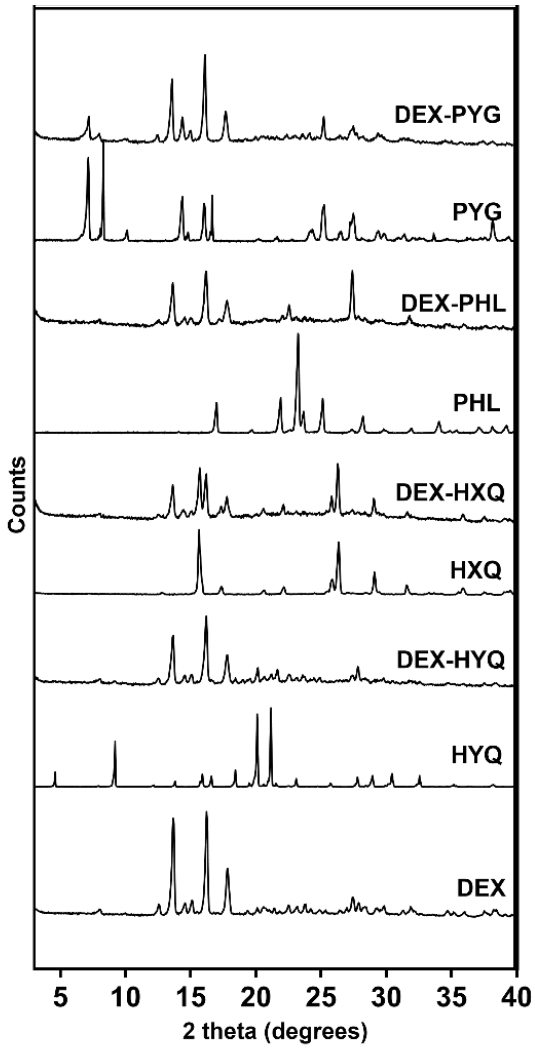

Fig. S3 PXRD patterns of the 1:1 physical mixture formed between DEX and HYQ/HXQ/PHL/PYG by neat grinding.

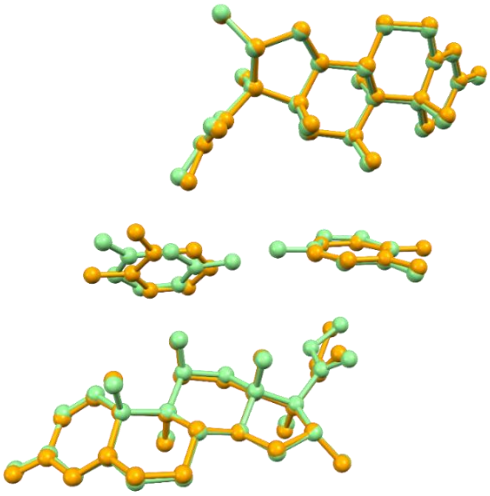

Fig. S4 Least-squares overlay (RMS = 0.0845 for six pairs of quaternary carbon atoms of DEX) of the structures of DEX-CAT (orange) and DEX-RES (light green). An additional pair of DEX (-x, ½+y, 1-z) and CAT (-x, -½+y, 1-z) molecules was generated for a better comparison with the asymmetric unit of DEX-RES.

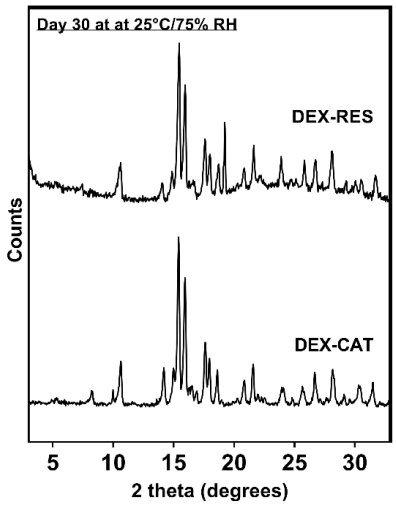

Fig. S5 Monitoring phase transformation of the DEX-benzenediol cocrystal systems by PXRD (1 month storage at 25°C/75% RH).

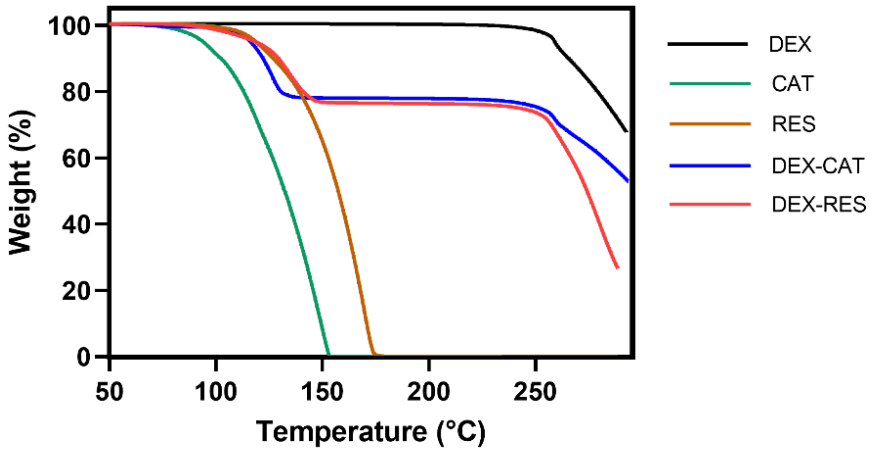

Fig. S6 TGA profiles of the DEX-benzenediol cocrystal systems, compared with the starting materials.

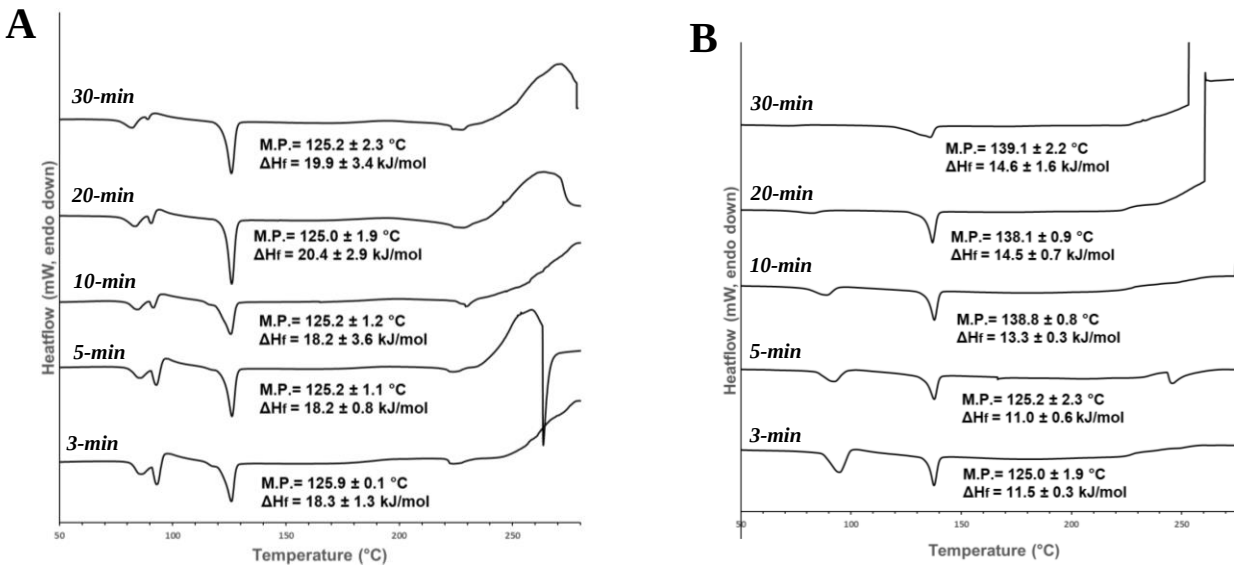

Fig. S7 Effect of grinding time on the thermal properties of DEX-CAT (A) and DEX-RES (B).

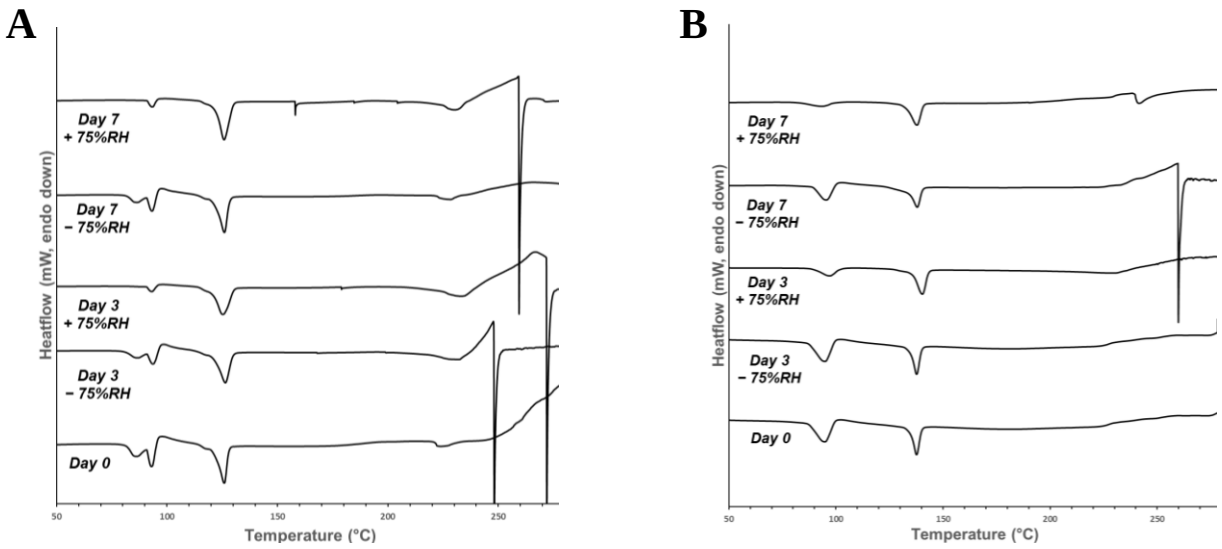

Fig. S8 Effect of annealing moisture (+75% RH) on recrystallization efficiency of the 3-min ground DEX-CAT (A) and DEX-RES (B). The controls (-75% RH) were stored in desiccator to prevent moisture absorption.

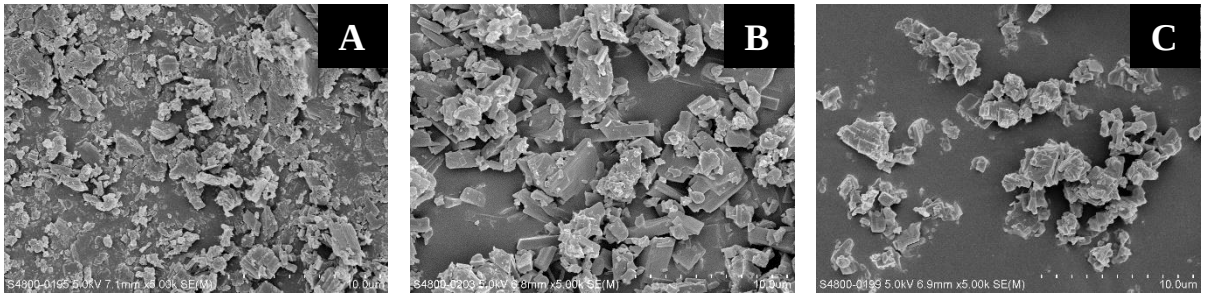

Fig. S9 SEM images of the sifted DEX (A), DEX-CAT (B), and DEX-RES (C) for the *in-vitro* drug release study, at 5000× magnification.

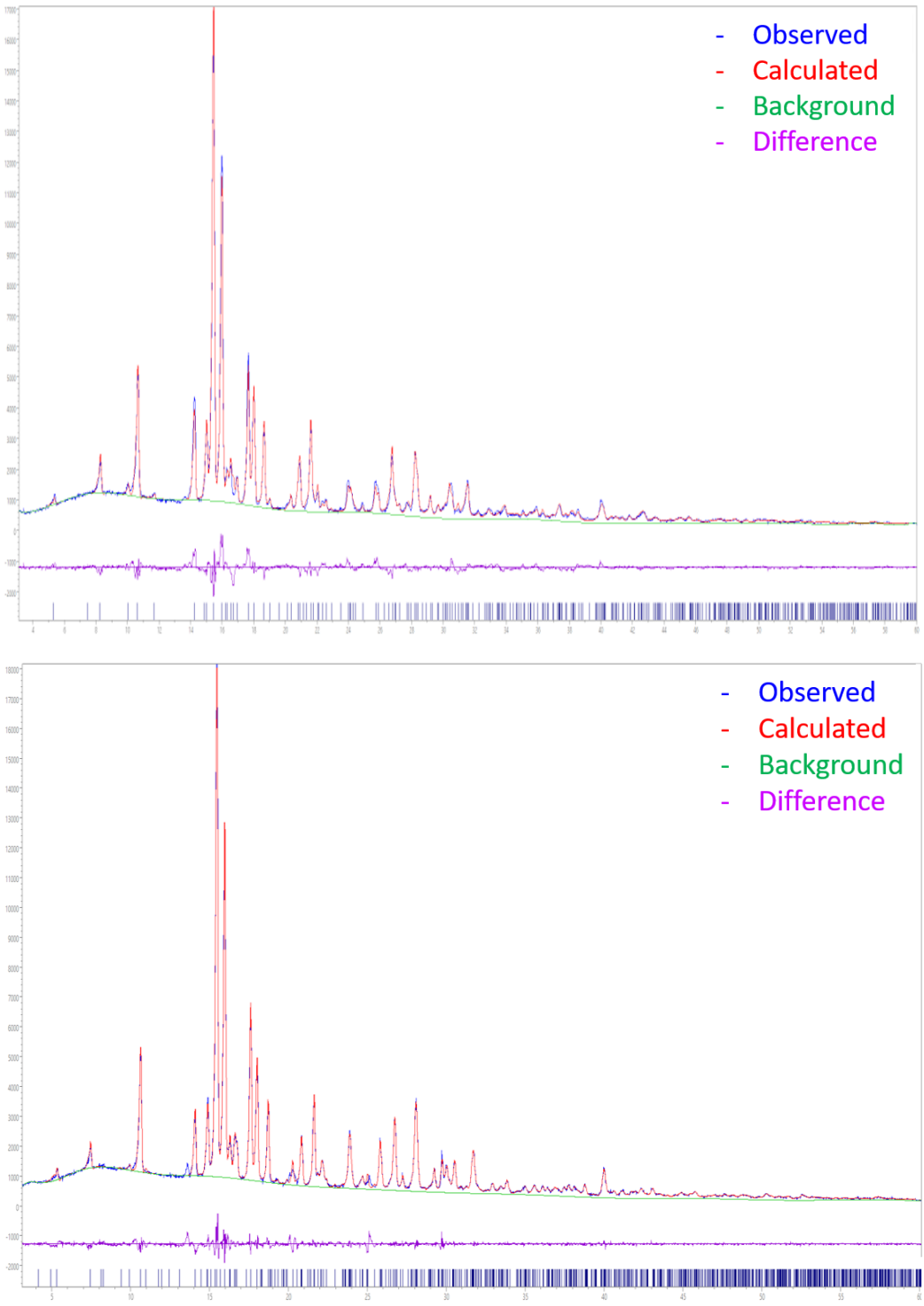

Fig. S10 The experimental data (blue), calculated pattern (red), background (green), and the difference between the experimental data and the calculated pattern (purple) profile plots of the Rietveld refinements of DEX-CAT (upper) and DEX-RES (lower).

References

1. A. Altomare, C. Giacovazzo, A. Guagliardi, A. G. Moliterni, R. Rizzi and P.-E. Werner, *J. Appl. Crystallogr.*, 2000, **33**, 1180-1186.
2. C. Brown, *Acta Crystallogr.*, 1966, **21**, 170-174.
3. G. Bacon and R. Jude, *Zeitschrift für Kristallographie-Crystalline Materials*, 1973, **138**, 19-40.
4. J. W. Raynor, W. Minor and M. Chruszcz, *Acta Crystallogr. Sect. Sect. E: Struct. Rep. Online*, 2007, **63**, o2791-o2793.
5. C. C. A. Altomare, C. Giacovazzo, A. Moliterni, R. Rizzi, N. Corriero and A. Falcicchio, *J. Appl. Cryst.* , 2013, 1231-1235.
6. L. Kürti, R. Gáspár, Á. Márki, E. Kápolna, A. Bocsik, S. Veszelka, C. Bartos, R. Ambrus, M. Vastag and M. A. Deli, *Eur. J. Pharm. Sci.*, 2013, **50**, 86-92.
7. S. A. Mohamad, A. M. Badawi and H. F. Mansour, *Int. J. Pharm.*, 2021, **601**, 120600.
8. C. Bartos, E. Pallagi, P. Szabó-Révész, R. Ambrus, G. Katona, T. Kiss, M. Rahimi and I. Csóka, *Eur. J. Pharm. Sci.*, 2018, **123**, 475-483.
9. M. Jug, A. Hafner, J. Lovrić, M. L. Kregar, I. Pepić, Ž. Vanić, B. Cetina-Čižmek and J. Filipović-Grčić, *J. Pharm. Biomed. Anal.*, 2018, **147**, 350-366.
10. M. Jug, A. Hafner, J. Lovrić, M. Lusina Kregar, I. Pepić, Ž. Vanić, B. Cetina-Čižmek and J. Filipović-Grčić, *ADMET and DMPK*, 2017, **5**, 173-182.
11. P. R. Spackman, M. J. Turner, J. J. McKinnon, S. K. Wolff, D. J. Grimwood, D. Jayatilaka and M. A. Spackman, *J. Appl. Crystallogr.*, 2021, **54**, 1006-1011.